Available online at www.sciencedirect.com
SCIENCE DIRECT®
Journal of Membrane Science 225 (2003) 177–186
journal of MEMBRANE SCIENCE
www.elsevier.com/locate/memsci

Pore size and surface chemistry effects on the transport of hydrophobic and hydrophilic solvents through mesoporous γ-alumina and silica MCM-48

Sankhanilay Roy Chowdhury, Riaan Schmuhl, Klaas Keizer, Johan E. ten Elshof*, Dave H.A. Blank

Department of Science and Technology, Inorganic Materials Science group, MESA+ Research Institute, University of Twente, P.O. Box 217, 7500 AE Enschede 7500, The Netherlands

Received 30 January 2003; received in revised form 25 June 2003; accepted 8 July 2003

Abstract

The structural and solvent transport properties of supported mesoporous γ-alumina and MCM-type silica membranes are reported. Templated mesoporous silica layers and powders were characterized by XRD, permporometry, XPS and BET measurements. The results indicate that the γ-alumina membrane is ∼1 μm thick, while the silica membrane is ∼30 nm thick, has a pore size of 2.8–3.4 nm and possesses the MCM-48 structure. Pressure-driven solvent flow experiments on α-alumina supported γ-alumina and MCM-48 membranes indicate that the permeabilities of the mesoporous layers depend on the chemical nature of the solvents. The permeability of hexane and toluene through γ-alumina with 4.5–7.5 nm pores is lower than that of hydrophilic alcohols and water. The permeability of water and alcohols through MCM-48 appears to be affected by solvent–pore interactions on molecular scale. The MCM-48 layer has a higher permeability than γ-alumina, which can be attributed to its much smaller thickness.

Keywords: Membrane; Gamma alumina; Silica; MCM-48; Permeability

1. Introduction

Nanofiltration (NF) membranes can be used to separate solvents from multivalent ions and small organic molecules. The separation through these membranes is thought to be controlled by a combination of size and charge effects. Sandwich-type ceramic composite membranes with NF characteristics typically have pore radii in the range of 0.5–3.5 nm [1,2]. The surface charge of the pores depends upon pH and can be either positive or negative, depending on the pH relative to the iso-electric point (IEP) of the oxide surface. Under moderate process conditions the pore size and structure of ceramic membranes is fixed. Inorganic NF membranes have been prepared from γ-alumina [1,3], titania [4,5], and silica–zirconia [6,7], and were employed for the rejection of large organic molecules [7], and the retention of small [5,6] and complex ions [3].

Although solvent permeation through polymeric NF membranes has been demonstrated successfully in many cases [8–11], one of the advantages of inorganic membranes is their resistance to virtually all solvents. The permeation of pure alcohols as non-aqueous solvents through inorganic membranes

* Corresponding author. Tel.: +31-53-489-2695; fax: +31-53-489-4683.
E-mail address: j.e.tenelshof@utwente.nl (J.E. ten Elshof).

0376-7388/$ – see front matter © 2003 Elsevier B.V. All rights reserved.
doi:10.1016/j.memsci.2003.07.018

has been discussed in detail [12], but only very few papers to date have reported on the application of inorganic nanofiltration membranes to separations of non-aqueous solutions, one exception being a separation process in a supercritical medium [4].

One of the main disadvantages of conventional inorganic membranes such as γ-alumina is the wide pore size distribution and the high tortuosity of the separating layer, which affects the intrinsic separation selectivity and permeability negatively. These disadvantages may be overcome by employing template-directed synthesis methods for the formation of the mesoporous top layer. A well-known example of a templated inorganic material is mesostructured silica, which is one of the major members of a larger class of mesoporous inorganic materials with long-range ordered pores. Templated silicas can be synthesized using arrays of self-assembled surfactant molecules as structure directing templates, around which the inorganic precursor species are polymerized [13]. Depending upon surfactant concentration and processing conditions, the final pore structure of silica will exhibit hexagonal, cubic or lamellar symmetry, which are denoted as MCM-41, MCM-48 and MCM-50, respectively [13,14]. In view of their high porosity and well-ordered pore geometries with narrow pore size distributions and low tortuosities, thin films of templated mesoporous materials are potential candidates for membrane applications. Although thin film formation on dense substrates has received considerable attention lately [15,16], only few works on film formation on porous supports have been reported to date [17–22].

The principal disadvantage of the 2D hexagonal MCM-41 structure for membrane applications is that the surfactant assemblies tend to align themselves parallel to the membrane interfaces during synthesis, which finally results in ordered pore structures with main transport paths parallel to the substrate. This geometric feature does not add any value to the improvement of tortuosity of porous thin films in the direction perpendicular to the membrane surface. Cubic MCM-48 on the other hand has an interconnected 3D channel system [23], so that a low tortuosity in all directions is expected. This feature should lead to a high permeability of the layer.

Although our final aim is to apply mesoporous ceramic membranes in nanofiltration applications, we limit the scope in the present work to the characterization of the transport behavior of several liquids (both hydrophobic and hydrophilic) through two different inorganic membranes, i.e. a conventional supported mesoporous γ-alumina membrane and a supported mesostructured silica MCM-48 membrane.

2. Experimental

2.1. Preparation of α-alumina supported mesoporous γ-alumina membrane

The γ-alumina membrane consists of a macroporous α-alumina support and a thin mesoporous γ-alumina layer. The α-alumina supports were made by colloidal filtration of well-dispersed 0.4 μm α-alumina particles (AKP-30, Sumitomo). The dispersion was stabilized by peptizing with nitric acid. After drying at room temperature, the filter compact was sintered at 1100 °C. Flat disks of ∅ 39 mm and 2.0 mm thickness were obtained after machining and polishing. The final porosity of these supports is ∼30% and the average pore size is in the range of 80–120 nm. Mesoporous γ-alumina membranes of ∼0.5 μm thickness were prepared by dip-coating the above-mentioned porous α-alumina supports in a boehmite sol, followed by drying and calcining at 600 °C for 1 h (heating/cooling rates 0.5 °C/min) [3].

2.2. Preparation of supported surfactant-templated mesoporous silica membrane

Surfactant-templated silica sols were synthesized using the cationic surfactant cetyl-trimethyl-ammonium bromide (CTAB, Aldrich) and tetraethoxy-orthosilicate (TEOS, Aldrich) derived sols as described elsewhere [24]. The required amount of TEOS was mixed with 1-propanol and stirred for 5 min. TEOS was then hydrolyzed at pH 2.5 by addition of an aqueous HCl solution. The solution was stirred for 1 h. 2-Butanol was added to the hydrolyzed sol and stirring continued for another 30 min. The surfactant solution was prepared separately and slowly added to the sol while stirring. A typical sol formulation was TEOS:1-propanol:2-butanol:H_2O:HCl(N) = 8:17.47:8.75:6.63:0.33 ml and TEOS:CTAB = 7.62:1. Spin-coating and dip-coating techniques were

used to deposit thin silica films on silicon wafers (004 type) and α-alumina supports, respectively. After coating the layers were dried at room temperature and heated to 450 °C in air for 2 h (heating/cooling rates 0.5 °C/min) to calcine the silica film and remove any residual organics.

X-ray photoelectron spectra (XPS) and depth profiles of the elemental composition of silica films were made using a PHI Quantum 2000 Scanning ESCA Microprobe. X-ray diffraction (XRD) patterns of supported silica layers were recorded using a Philips SR5056 with Cu Kα radiation. BET measurements (Micromiretics) were performed at 77 K on dried and calcined silica powders with N_2 as the condensable gas.

2.3. Solvent permeation experiments

Steady state liquid flux measurements were carried out using water, ethanol, 1-propanol, 2-butanol, toluene and hexane in a dead-end nanofiltration cell on α-alumina supports, supported γ-alumina composite membranes and supported mesoporous silica membranes. The volume of the cell is 700 ml and the operating pressure range was kept in the range of 2–14 bar [3]. The stirring speed in the cell was kept constant at 209.44×10^{-1} rad/s (200 rpm) throughout all experiments. Subsequent liquid permeation experiments on the same membrane were carried out in a sequence that started with the most hydrophobic (hexane) and ended with the most hydrophilic (water) solvent. Prior to the experiments, the supported membranes were left over night in 2-propanol to leach out any condensed water from the membrane mesopores. It was not necessary to carry out this pre-treatment step for the permeation experiments on bare α-alumina supports.

3. Results and discussion

3.1. Characterization of the templated silica membrane

Fig. 1 shows a small angle XRD pattern of a 100 nm thick uncalcined silica film after deposition on a dense silicon wafer. The X-ray pattern matches the pattern of an ordered mesoporous MCM-48 phase with unit cell $a \sim 9.2$ nm [25]. The marked

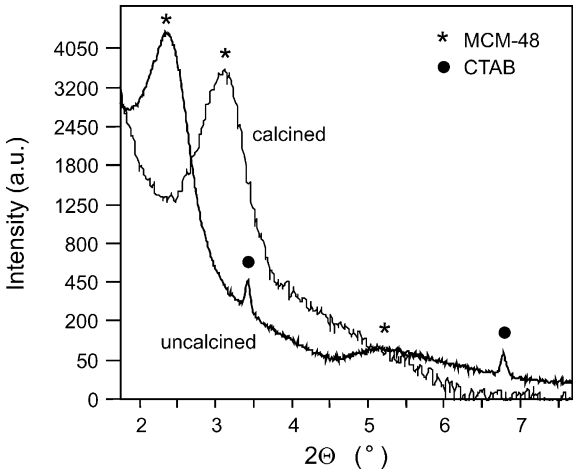

Fig. 1. XRD diagrams of uncalcined air-dried and calcined silica layer on silicon (0 0 4) wafer.

sharp peaks are probably from crystalline CTAB and they disappear upon calcination. The sample retains its mesostructure after calcination but with smaller *d*-spacings (Fig. 1, $a \sim 6.3$ nm). We did not observe diffraction at low angles in the films that had been deposited on porous α-alumina supports. This is likely due to the roughness and texture of the alumina support, which promotes local nucleation and growth of ordered domains with different orientations at length scales that are probably too small to be detectable by XRD. Moreover, the XPS depth profile of an alumina supported MCM-48 membrane shows only a very thin silica film (20–30 nm), as illustrated in Fig. 2. Permporometry experiments with cyclohexane [26] on the alumina-supported MCM-48 membrane indicated that the calcined silica films are porous and defect-free. The Kelvin radius of all pores was below the experimental lower limit of ∼1.7 nm of the permporometry method. However, this agrees with nitrogen sorption data on unsupported MCM-48 powder, from which an average pore diameter of 2.8–3.4 nm was calculated.

3.2. Liquid permeation through macroporous α-alumina support

Fig. 3 shows the volume liquid flux as a function of pressure. The volume flux at steady state is proportional to the applied pressure, which indicates that

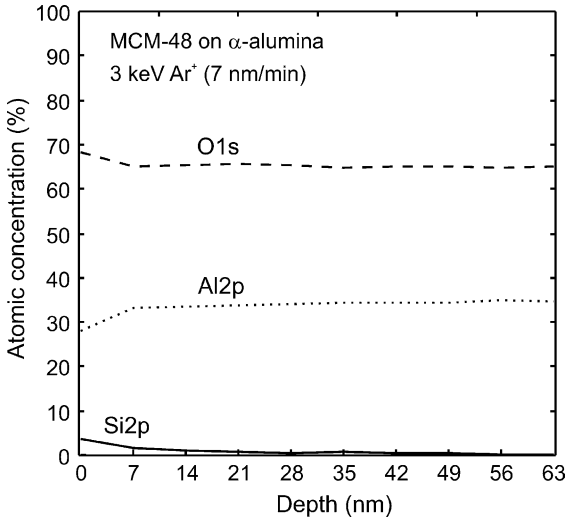

Fig. 2. XPS depth profile of calcined silica MCM-48 membrane on porous α-alumina support.

pressure difference is the only driving force for the permeation of solvents. When the transport mechanism obeys the viscous flow model, the flux versus pressure plot can be expressed as a straight line that goes through the origin, irrespective of the type of liquid (Darcy's law). In Fig. 3 it can be seen that the liquid flux through the support decreases with increasing viscosity of the solvent according to

$$J = -\frac{1}{\eta} k_{\mathrm{m}} \Delta P \tag{1}$$

where J is the flux, η the bulk liquid viscosity, ΔP the applied pressure gradient across the membrane, and k_{m} the overall membrane permeability. This is further illustrated in Fig. 4, which shows the product of flux and solvent viscosity as a function of applied pressure. It is clear from this figure that the flux through α-alumina membranes with a pore diameter of ∼100 nm is only influenced by applied pressure and solvent viscosity, as is expected for macroporous systems. A linear fit to the data of Fig. 4 yields a value $k_{\mathrm{m}} = (1.17 \pm 0.08) \times 10^{-14}$ m for the permeability of the α-alumina layer.

3.3. Solvent permeation through supported γ-alumina membrane

The pore size distribution of the γ-alumina membrane as determined by permporometry is shown in Fig. 5. The Kelvin radius is 2–3.5 nm. Fig. 6 shows the fluxes of several liquids through a composite γ-alumina membrane. In general, when the pores of the γ-alumina layer were pre-filled with a certain solvent, the permeation of a more hydrophilic solvent could be initiated easily upon applying a low pressure,

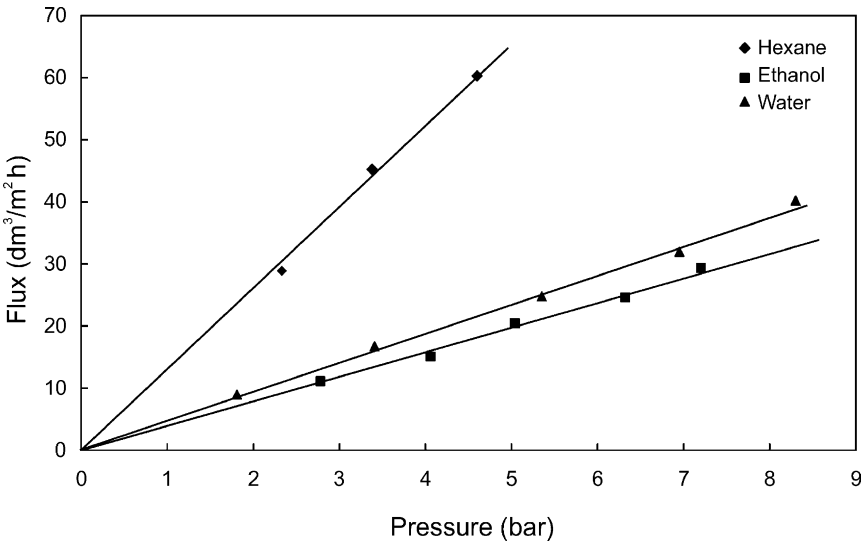

Fig. 3. Solvent fluxes through α-alumina support.

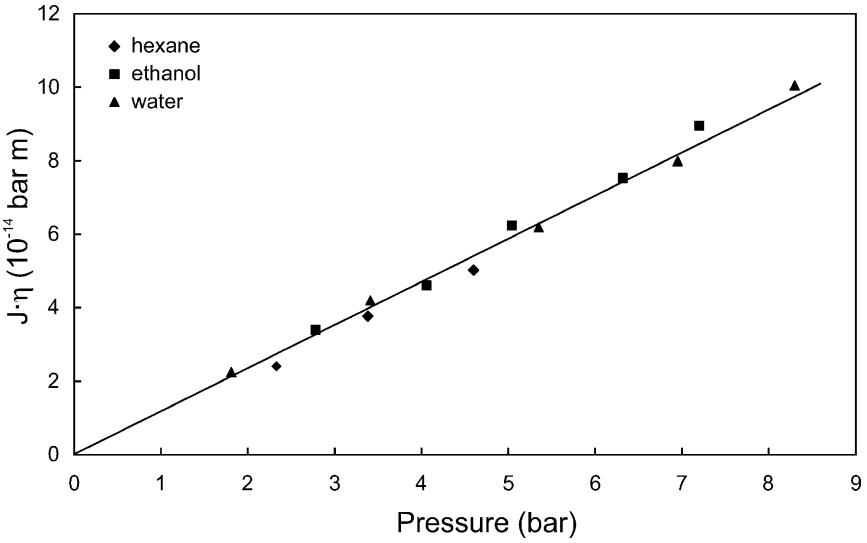

Fig. 4. Viscosity-corrected fluxes through α-alumina support.

while initiation of liquid transport of a more hydrophobic solvent required a very high pressure. This was attributed to the higher affinity that hydrophilic liquids have for the (hydrophilic) γ-alumina matrix in comparison with hydrophobic liquids. For this reason, transport experiments with different solvents were always carried out in a sequence that started with the most hydrophobic (hexane) and ended with the most hydrophilic (water) solvent. The figure indicates that water passes most easily through the membrane at a given pressure. As for the α-alumina support, the flux decreases with increasing solvent viscosity. Fig. 7 presents the same liquid fluxes through γ-alumina after correction for differences in solvent bulk viscosity. Some remarkable features can be observed in this figure. In contrast to macroporous α-alumina, the transport of solvents through mesoporous γ-alumina appears to depend on the chemical nature of the

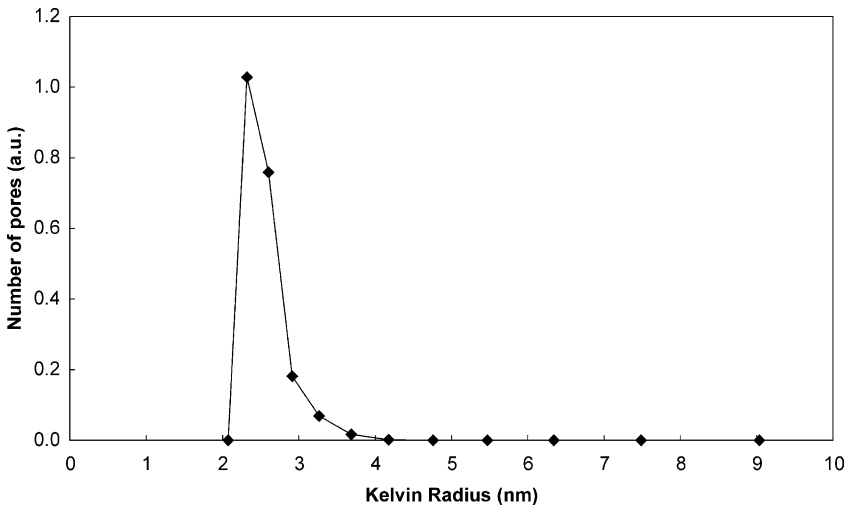

Fig. 5. Pore size distribution of γ-alumina membrane determined by permporometry.

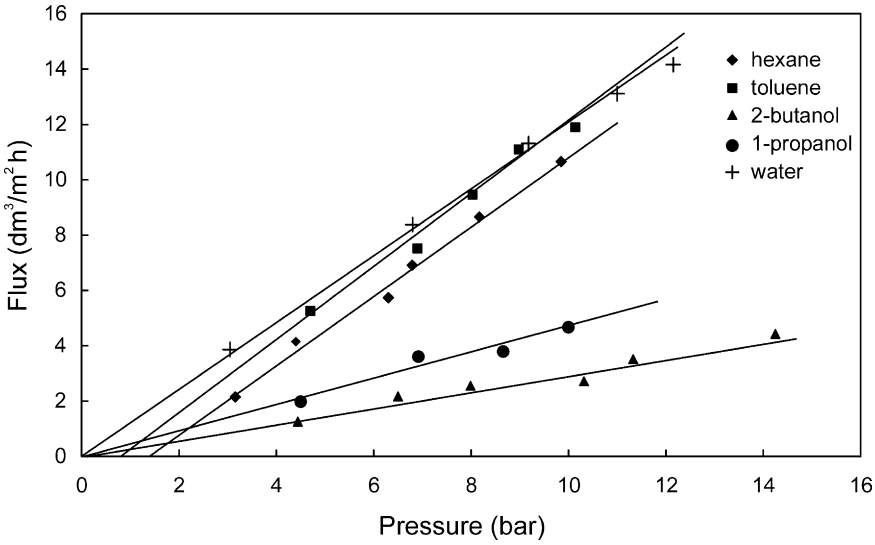

Fig. 6. Solvent fluxes through supported γ-alumina membrane.

solvent. The hydrophobic liquids have a considerably lower permeability than more hydrophilic alcohols and water. This indicates that the small pore size of γ-alumina influences the permeability of liquids with different chemical nature. Linear fits of the flux data shown in Fig. 7 indicate that water and alcohols have a zero flux at zero applied pressure, i.e. these liquids appear to follow Darcy's law even when they are transported through the narrow γ-alumina pores of 4.5–7.5 nm diameter. In contrast, the hydrophobic liquids toluene and hexane require a certain threshold pressure before transport through the hydrophilic pores of the γ-alumina membrane is observed. It is known that the behavior of liquids in confined geometries of only a few molecular diameter dimensions can deviate largely from the behavior of bulk liquids and is not understood in detail [27]. One possible explanation for the differences in permeability of hydrophilic and hydrophobic liquids may be related to differences in their wetting behavior inside narrow

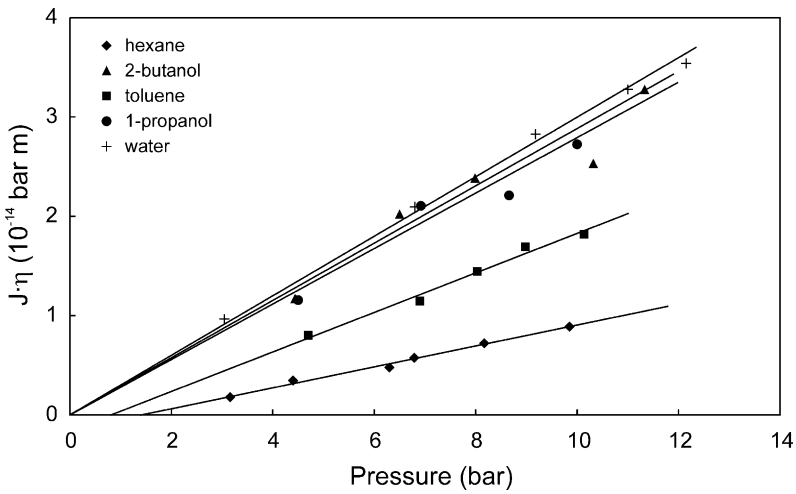

Fig. 7. Viscosity-corrected fluxes through supported γ-alumina membrane.

pores. Hydrophilic liquids will wet the internal pore surface easily due to the favorable hydrogen bond interactions between the liquid and the hydrophilic γ-alumina surface. These liquids may therefore use the entire cross-sectional area of the membrane pore for transport. On the other hand, hydrophobic liquids may tend to stay away from the γ-alumina interface due to unfavorable hydrophobic-hydrophilic interactions. Such molecules may therefore use less of the cross-sectional area of the membrane pores for flow, i.e. the effective pore size is smaller in this case, which decreases the permeabilities of such liquids. However, there are probably several alternative or additional factors involved, such as differences in molecular size, rigidity of the solvent molecules and/or near-surface ordering phenomena.

It is clear from Fig. 6 that hexane and toluene both need a certain threshold pressure to be exceeded before flow through the γ-alumina layer commences. The approximate values of the threshold pressures are listed in Table 1. The reasons for a non-zero threshold pressure are not clear. Toluene appears to have a slightly lower threshold pressure than hexane, which might be explained by the more favorable interactions between the electron clouds of the aromatic ring of toluene with the charged γ-alumina surface at very small distances. This may facilitate toluene to enter and wet the pore in comparison with hexane.

The overall transport resistance of liquids through a stacked membrane can be regarded as a series of two transport resistances in series. The overall membrane permeability k_m can be therefore be deconvoluted into the permeabilities of the individual layers according to

$$\frac{1}{k_m} = \frac{1}{k_\alpha} + \frac{1}{k_\beta}, \quad (2)$$

Table 1
Permeabilities and threshold pressures for mesoporous γ-alumina and MCM-48 layers

Solvent	k_β (10^{-14} m)		Threshold pressure (bar)
	γ-Alumina	MCM-48	
Water	0.40 ± 0.06	22 ± 3.1	0
Ethanol		10–20	0
1-Propanol	0.35 ± 0.07	6.9 ± 1.3	0
2-Butanol	0.37 ± 0.08		0
Toluene	0.24 ± 0.07		0.8 ± 0.4
Hexane	0.11 ± 0.02		1.4 ± 0.7

where k_α and k_β are the permeabilities of the α-alumina support and the mesoporous top layer, respectively. Table 1 summarizes the k_β values of the γ-alumina top layer for several solvents. The k_β values of water and alcohols are the same within experimental error, while those of hexane and toluene are substantially smaller.

3.4. Solvent permeation through supported MCM-48 membrane

Figs. 8 and 9 show directly measured and viscosity-corrected fluxes of several hydrophilic liquids for the supported MCM-48 membrane. Unlike γ-alumina, the permeabilities of different hydrophilic alcohols are different. The permeability reduces upon going from water to 1-propanol. It is noted that the pore size of MCM-48 (∼3 nm) is substantially smaller than that of γ-alumina (4.5–7.5 nm), which may indicate that specific interactions between solvent molecules and the MCM-48 surface become significant at these small pore sizes. The variation between different liquids can probably be attributed to differences in hydrophobic–hydrophilic interactions between the pore walls and the solvents, and/or to alkoxylation of surface ≡Si–OH groups by ethanol and 1-propanol, which yields ≡Si–OR surface groups (R = C_2H_5, C_3H_7) that are somewhat bulkier than ≡Si–OH groups [28]. Alkoxylation may therefore reduce the effective pore radius, resulting in an effectively smaller cross-sectional pore area and therefore a lower permeability for higher alcohols. This effect is reflected in the permeabilities k_β of the MCM-48 layer listed in Table 1. The k_β data of MCM-48 are estimated values, as the overall resistance of the stacked membrane is determined primarily by the resistance $1/k_\alpha$ of the α-alumina support. For the specific experiments with water and ethanol shown in Fig. 9, the resistance of the MCM-48 layer was even negligible in comparison with the resistance of the support.

The silica MCM-48 membrane shows much higher liquid fluxes than the γ-alumina membrane for similar liquids, and the permeability k_β of the MCM-48 layer is higher as well. However, these differences can be explained largely by taking into account that the MCM-48 layer is much thinner than the γ-alumina layer (∼30 and ∼500 nm, respectively). A measure for the intrinsic permeability of the mesoporous

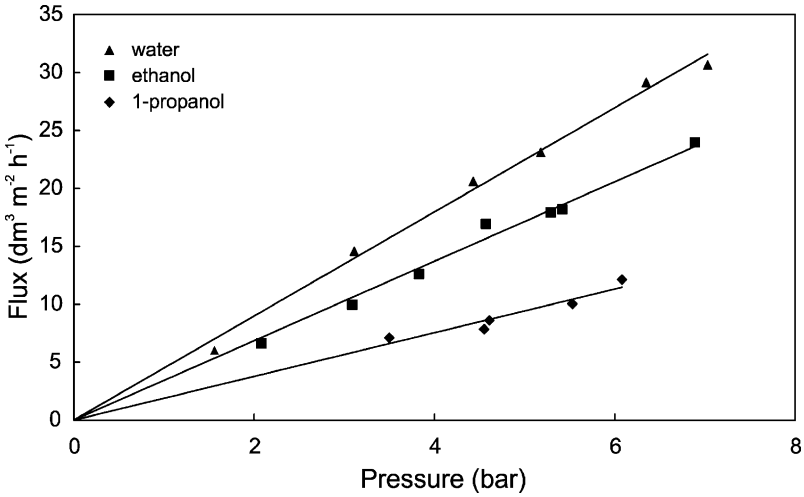

Fig. 8. Solvent fluxes through supported silica MCM-48 membrane.

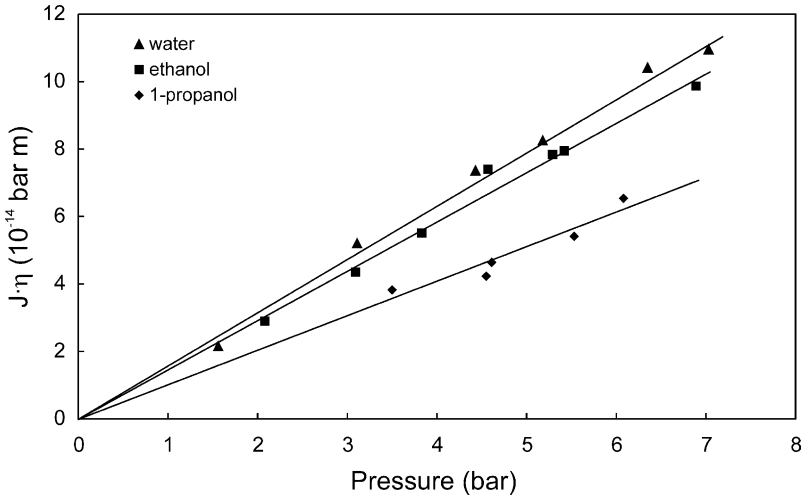

Fig. 9. Viscosity-corrected fluxes through supported silica MCM-48 membrane.

structure is given by the product $k_\beta L_\beta$, where L_β is the thickness of the mesoporous layer. Upon comparing the $k_\beta L_\beta$ values of γ-alumina and MCM-48, it appears that $k_\beta L_\beta$ is still approximately a factor of 1.2-3 higher for MCM-48 (depending on the type of solvent). Most likely this can be attributed to differences in porosity and tortuosity of the two systems: γ-alumina has a porosity of 40–50% and a high tortuosity of 5–15 [29], while the porosity of MCM-48 is >60% [30], and the tortuosity of MCM-type materials is smaller than 3 [31].

4. Conclusions

Mesoporous silica MCM-48 layers can be deposited defect-free in 30 nm thick layers on/into macroporous α-alumina supports. The transport resistance of the resulting stacked α-alumina/MCM-48 membrane is dominated by the transport resistance of the support. In contrast, γ-alumina is normally applied in 500–1000 nm thick layers, and it was shown that the resistance of this layer contributes significantly to the overall transport resistance. The higher permeability

of MCM-48 layer in comparison with γ-alumina can be accounted for mainly by the difference in layer thickness.

Pressure-driven solvent flow experiments on α-alumina supported γ-alumina and MCM-48 membranes indicate that the permeability of the mesoporous layers is influenced by the chemical nature of the liquids. This feature opens up possibilities to apply mesoporous inorganic membranes for the separation of immiscible solvents or the removal of traces of hydrophilic liquids from hydrophobic solvents.

Depending on ambient conditions, the mesopores of γ-alumina and MCM-48 are often blocked by condensed water, which cannot be removed easily by hydrophobic solvents even when pressures up to 15–20 bar are applied. For permeation of hydrophobic solvents it is therefore necessary to pre-treat the membrane with a solvent in which water can dissolve well, and that is soluble in the hydrophobic solvent that has to be transported.

The small pore size and narrow pore size distribution of MCM-48 are promising features for achieving high selectivity in size- and charge-based nanofiltration processes.

Acknowledgements

Financial support of the Commission of the EC in the framework of the Growth Programme, contract no. G1RD-2000-00347 (SUSTOX), is gratefully acknowledged.

References

[1] A. Larbot, S. Alami-Younissi, M. Persin, J. Sarrazin, L. Cot, Preparation of α-alumina nanofiltration membrane, J. Membr. Sci. 97 (1994) 167.

[2] W.B.S. de Lint, Transport of electrolytes through ceramic nanofiltration membranes, Ph.D. Thesis, University of Twente, The Netherlands, 2003.

[3] S. Roy Chowdhury, J.E. ten Elshof, N.E. Benes, K. Keizer, Development and comparative study of different nanofiltration membranes for highly charged large ion recovery, Desalination 144 (2002) 41.

[4] S. Sarrade, G.M. Rios, M. Carles, Nanofiltration membrane behavior in a supercritical medium, J. Membr. Sci. 114 (1996) 81.

[5] G.M. Rios, R. Joulie, S.J. Sarrade, M. Carles, Investigation of ion separation by microporous nanofiltration membranes, AIChE J. 42 (1996) 2521.

[6] T. Tsuru, H. Takezoe, M. Asaeda, Ion separation by porous silica–zirconia nanofiltration membranes, AIChE J. 44 (1998) 765.

[7] T. Tsuru, S. Wada, S. Izumi, M. Asaeda, Silica–zirconia membranes for nanofiltration, J. Membr. Sci. 149 (1998) 127.

[8] D.R. Machado, D. Hasson, R. Semiat, Effect of solvent properties on permeate flow through nanofiltration membranes. Part I. Investigation of parameters affecting solvent flux, J. Membr. Sci. 163 (1999) 93.

[9] X.J. Yang, A.J. Livingston, L. Freitas dos Santos, Experimental observations of nanofiltration with organic solvents, J. Membr. Sci. 190 (2001) 45.

[10] D. Banushali, S. Kloos, C. Kurth, D. Bhattacharyya, Performance of solvent-resistant membranes for non-aqueous systems: solvent permeation results and modeling, J. Membr. Sci. 189 (2001) 1.

[11] D.R. Machado, D. Hasson, R. Semiat, Effect of solvent properties on permeate flow through nanofiltration membranes, J. Membr. Sci. 166 (2000) 63.

[12] T. Tsuru, T. Sudou, S. Kawahara, T. Yoshioka, M. Asaeda, Permeation of liquids through inorganic nanofiltration membranes, J. Colloid Interface Sci. 228 (2000) 292.

[13] J.S. Beck, J.C. Vartuli, W.J. Roth, M.E. Leonowicz, C.T. Kresge, K.D. Schmitt, C.T.-W. Chu, D.H. Olson, E.W. Sheppard, S.B. McCullen, J.B. Higgins, J.L. Schlenkert, A new family of mesoporous molecular sieves prepared with liquid crystal templates, J. Am. Chem. Soc. 114 (1992) 10834.

[14] D. Zhao, J. Feng, Q. Huo, N. Melosh, G. Fredrickson, B. Chmelka, G.D. Stucky, Triblock copolymer syntheses of mesoporous silica with periodic 50 to 300 angstrom pores, Science 279 (1998) 548.

[15] D. Zhao, P. Yang, N. Melosh, J. Feng, B.F. Chmelka, G.D. Stucky, Continuous mesoporous silica films with highly ordered large pore structures, Adv. Mater. 10 (1998) 1380.

[16] H. Yang, N. Coombs, I. Sokolov, G.A. Ozin, Registered growth of mesoporous silica films on graphite, J. Mater. Chem. 7 (1997) 1285.

[17] D. Zhao, P. Yang, D.I. Margolese, B.F. Chmelka, G.D. Stucky, Synthesis of continuous mesoporous silica thin films with three-dimensional accessible pore structures, Chem. Commun. (1998) 2499.

[18] M. Klotz, A. Ayral, C. Guizard, L. Cot, Synthesis and characterization of silica membranes exhibiting an ordered mesoporosity. Control of the porous texture and effect on the membrane permeability, Sep. Purif. Tech. 25 (2001) 71.

[19] D.-H. Park, N. Nishiyama, Y. Egashira, K. Ueyama, Enhancement of hydrothermal stability and hydrophobicity of a silica MCM-48 membrane by silylation, Ind. Eng. Chem. Res. 40 (2001) 6105.

[20] Y.-S. Kim, S.-M. Yang, Preparation of continuous mesoporous silica thin film on a porous tube, Adv. Mater. 14 (2002) 1078.

[21] K.J. Edler, S.J. Roser, Growth and characterization of mesoporous silica films, Int. Rev. Phys. Chem. 20 (2001) 387.

[22] M. Klotz, S. Besson, C. Ricolleau, F. Bosc, A. Ayral, Ordered 3D hexagonal mesoporous silica membranes: synthesis and characterization, in: V.N. Burganos, R.D. Noble, M. Asaeda, A. Ayral, J.D. LeRoux (Eds.), MRS Proceedings, vol. 752, Materials Research Society, Warrendale, 2003.
[23] M.W. Anderson, Simplified description of MCM-48, Zeolites 19 (1997) 220.
[24] I. Honma, H.S. Zhou, D. Kundu, A. Endo, Structural control of surfactant-templated hexagonal, cubic, and lamellar mesoporous silicate thin films prepared by spin-casting, Adv. Mater. 12 (2000) 1529.
[25] J. Xu, Z. Luan, H. He, W. Zhou, L. Kevan, A reliable synthesis of cubic mesoporous MCM-48 molecular sieve, Chem. Mater. 10 (1998) 3690.
[26] G.Z. Cao, J. Meijerink, H.W. Brinkman, A.J. Burggraaf, Permporometry study on the size distribution of active pores in porous ceramic membranes, J. Membr. Sci. 83 (1993) 221.
[27] M.L. Gee, P.M. McGuiggan, J.N. Israelachvili, A.M. Homola, Liquid to solid like transitions of molecularly thin films under shear, J. Chem. Phys. 93 (1990) 1895.
[28] G.C. Ossenkamp, T. Kemmitt, J.H. Johnston, New approaches to surface-alkoxylated silica with increased hydrolytic stability, Chem. Mater. 13 (2001) 3975.
[29] A.F.M. Leenaars, A.J. Burggraaf, The preparation and characterization of alumina membranes with ultra-fine pores. Part 3. The permeability for pure liquids, J. Membr. Sci. 24 (1985) 245.
[30] M. Widenmeyer, R. Anwander, Pore size control of highly ordered mesoporous silica MCM-48, Chem. Mater. 14 (2002) 1827.
[31] C.E. Salmas, V.N. Stathopoulos, P.J. Pomonis, H. Rahiala, J.B. Rosenholm, G.P. Androutsopoulos, An investigation of the physical structure of MCM-41 novel mesoporous materials using a corrugated pore structure model, Appl. Catal. A 216 (2001) 23.